ChemistryEurope
Excellence in Chemistry Research Worldwide

Research Article
doi.org/10.1002/ceur.202300021

www.journal.chemistry-europe.org

N-Doped Octagon-Containing HBC as Redox and pH Chiroptical Switch in the NIR

Miguel A. Medel,[a] Lidia Hortigüela,[a] Vega Lloveras,[b] José Catalán-Toledo,[b] Delia Miguel,[c] Antonio J. Mota,[d] Núria Crivillers,*[b] Araceli G. Campaña,*[a] and Sara P. Morcillo*[a]

The optical and chiroptical properties of an aza-HBC-*oct*-[5]helicene have been studied and also modulated by means of protonation or oxidation. In both cases, the generated species shows a new absorption band in the NIR region that is not present in the neutral species. This result enables this N-doped nanographene to act both as optical and, remarkably, as chiroptical switch since both the CD and CPL can be modulated by external stimuli such as redox or pH changes.

Introduction

The scientific community is putting considerable effort in developing methods to synthesize nanographenes controlling both the shape and the introduction of defects.[1] This control allows to tune the electronic, optical and chiroptical properties of the nanographenes, which is crucial to provide molecular materials potentially used in new applications in the field of organic electronics,[2] such as chiroptical switches[3] and spin filters.[4] The common defects introduced in nanographenes are helicenes, non-hexagonal rings, doping with heteroatoms or a combination of the previous defects.[5] They often lead to the formation of chiral non-planar systems. In this sense, our research group has recently reported new strategies for the insertion of non-hexagonal rings (heptagonal,[6] octagonal[7] and nonagonal[8] rings) into both the helicene and the hexa-*peri*-hexabenzocoronene (HBC) unit, which is the prototypical nanographene molecule. This strategy of combining two defects in the same compound leads to chiral helical nanographenes with high configurational stability[9] and interesting chiroptical properties,[10] reaching values of g_{lum}, the dissymmetry factor of circularly polarized luminescence (CPL), up to 2×10^{-3}.[11] Therefore, we wonder if the introduction of nitrogen atom as a third defect into a HBC could have a significant impact in the resulting properties and their modulation.

It is well known that the incorporation of heteroatoms in polycyclic aromatic systems changes significantly their electronic or magnetic properties.[12] In particular, the π-conjugation on the graphenic structures can be modulated by nitrogen doping due to the lone pair of electrons provided.[13] It also allows the coordination with metals[14] or protons,[15,16] which will lead to ligands in supramolecular structures or acid-responsive materials, respectively. For instance, it has been shown that the incorporation of pyrimidine[17] or pyridine[18] rings into the HBC skeleton not only modifies the electronic properties but also allows the modulation of their properties with pH variations. Moreover, N-doping of HBCs can alter the hexagonal net when introducing non-hexagonal rings, such as pyrrole, and hence, its redox properties.[19] In this regard, K. Müllen et al. obtained hexapyrrolohexaazacoronenes (HPHAC) and the corresponding dicationic species after chemical oxidation making them of interest as an electrochromic molecule.[20] It has also been demonstrated that the π-extension of the HPHAC motif can lead to the formation of heptagonal rings which result in a considerable red shifted absorption of the neutral and the cationic states.[19a] More interestingly, the combination of octagonal carbocycles with N-doping leads to high configurationally stable nanographenes enabling to study their chiroptical properties. One example is the triaza monkey saddle structure reported by the group of M. Mastalerz.[21] In another interesting example, reported by M. Melle-Franco, A. Mateo-Alonso et al., the octagonal ring stabilizes the helical conformation of a molecular nanoribbons.[22] Recently, the group of P. An et al.[23] has reported the aza-HBC-*oct*-[5]helicene version of our previously reported HBC-*oct*-[5]helicene.[7] Despite these advances, to the best of our knowledge, the system

[a] Dr. M. A. Medel, L. Hortigüela, Prof. A. G. Campaña, Dr. S. P. Morcillo
Department of Organic Chemistry
Unidad de Excelencia de Química (UEQ),
Faculty of Sciences
University of Granada
Avda. Fuente Nueva s/n, 18071, Granada (Spain)
E-mail: araceligc@ugr.es
samorcillo@ugr.es

[b] Dr. V. Lloveras, J. Catalán-Toledo, Prof. N. Crivillers
Department of Molecular Nanoscience and Organic Materials
Institut de Ciència de Materials de Barcelona (ICMAB) / CIBER-BBN
Campus Universitari de Bellaterra, 08193, Cerdanyola, Barcelona (Spain)
E-mail: ncrivillers@icmab.es

[c] Prof. D. Miguel
Nanoscopy-UGR Laboratory. Physical Chemistry Department
UEQ, Faculty of Pharmacy
University of Granada
C. U. Cartuja, 18071, Granada (Spain)

[d] Prof. A. J. Mota
Department of Inorganic Chemistry
UEQ, Faculty of Science
University of Granada
Avda. Fuente Nueva s/n, 18071 Granada (Spain)

Supporting information for this article is available on the WWW under https://doi.org/10.1002/ceur.202300021

Research Article
doi.org/10.1002/ceur.202300021

reported here is the first example in which the combination of non-planar HBC, N-doping and helicity in the same structure permits to tune its chiroptical properties by different stimuli. Indeed, such stimuli may generate new species that absorb or emit chiral light in the near-infrared region (NIR $>$780 nm. This NIR absorption is of great interest for many relevant applications,[24] such as in optical imaging to detect biological tissues.[25] Whilst several studies focused on chiroptical switching at UV-Vis region[26,27] of N-doped helicenoids have been reported, the modulation in the NIR region have only been achieved in metal-based helicenoids[28] (Figure 1). In this respect, herein, we go a step further and present the synthesis and characterization of chiral N-doped distorted nanographene and both the optical and the chiroptical properties are controlled by pH and redox stimuli, showing characteristic new bands in the NIR region that can be easily modulated without the need of using metals.

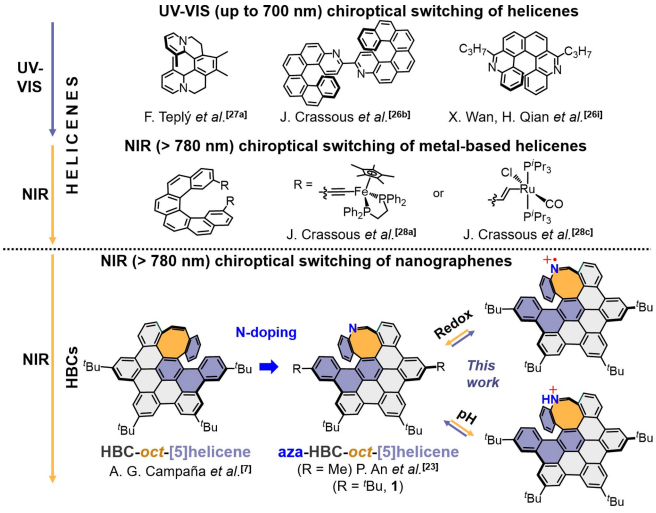

Figure 1. Top: selected previous examples of helical chiroptical switches in the UV-Vis (up to 700 nm) and in the NIR region (by metal interactions). Bottom: Previous (aza−)HBC-*oct*-[5]helicene and present N-doped analogue acting as redox and pH chiroptical switch in the NIR.

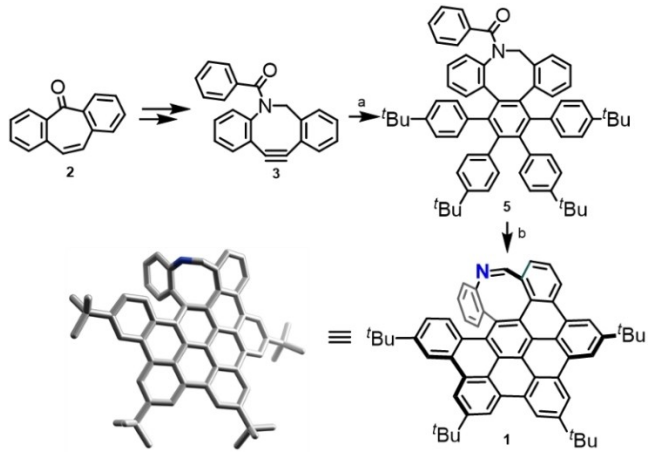

Scheme 1. Synthesis of **1**. Reagents and conditions. a) 2,3,4,5-tetrakis(4-(tert-butyl)phenyl)cyclopenta-2,4-dien-1-one (**4**), Ph_2O, reflux, 2 h, 70%; b) DDQ, CF_3SO_3H, CH_2Cl_2, 0 °C, 12 min, 28%. Bottom left: DFT optimized geometry of **1**.

Results and Discussion

The synthetic route towards aza-HBC-*oct*-[5]helicene **1** is similar to those previously reported,[7,23] which is based on the Beckmann rearrangement to insert the nitrogen atom and to expand the seven-membered ring of dibenzosuberenone **2** (Scheme 1). Afterwards, the aza-hexaphenylbenzene **5** was prepared by Diels-Alder reaction from the described aza-cyclobenzooctyne **3** and cyclopentadienone **4** (70%). Subsequently, oxidative cyclodehydrogenation of **5** using Rathore conditions (DDQ/CF_3SO_3H)[29] provided selectively **1** in a moderate yield (28%).

This N-doped nanographene is very soluble in common organic solvents, allowing its full characterization by means of ^{1}H- and ^{13}C NMR spectroscopy and HRMS. The position of the helicene was assigned by 2D NMR experiments (Figures S11–S14) and it is localized close to the nitrogen of the imine group. Unfortunately, we were not able to obtain suitable crystals of **1** for X-ray diffraction. Therefore, we carried out its geometrical optimization (DFT-CAM–B3LYP/6-31G(d,p)) leading to a highly distorted structure (Scheme 1, bottom left). The saddle curvature induced by the octagonal ring reaches 2.3 Å deep and the maximum dihedral angle described by the helicene (66.4°) is similar to the one observed for the all-carbon HBC-*oct*-[5]helicene (66.8°) previously reported by our research group (Figure 1, bottom left)[7] and the N-doped HBC-*oct*-[5]helicene (67.6°) reported by P. An et al.[23] In addition, the angle between the two planes described by the terminal rings of the [5]helicene of **1** (78.9°, Figure S25) is again in good agreement with the HBC-*oct*-[5]helicenes, slightly superior than other related analogues such as Rajca's *oct-[5]helicene* (72.4°)[30] or Narita's HBC-*hept-[5]helicene* (77.3°)[31] and, lower than the actual value of An's aza-HBC-*oct*-[5]helicene (87.4°). This difference might be due to the presence of different substituents.[23]

After its unequivocal characterization, the optical and electronic properties of **1** were investigated. The absorption spectra in CH_2Cl_2 (Figure 2, top, solid line), show a maximum at 351 nm ($\varepsilon = 8.5\times10^4$ M^{-1} cm^{-1}) in the same range as their all-carbon analogues and red-shifted compared with aza-[5]helicenes (261 nm), as expected from the larger π-extension of **1**.[32] The absorption onset corresponds to an optical band gap of 2.97 eV (417 nm, calculated from the crossing of the slope of the last absorption band with the abscissa axis), which is slightly higher than those found for HBC-*oct*-[5]helicenes. In addition, upon excitation at 370 nm, there is a broad emission band centered at 457 nm that is not red-shifted in comparison with all-carbon analogue (Figure 2, top, dashed line). The study of the fluorescence quantum yield (φ_F) in CH_2Cl_2 revealed that N-doping represents an improvement since **1** doubles the φ_F value (4%) compared with the fully carbonated HBC-*oct*-[5]helicene analogue (2%)[7] and also resulted higher than reported value by An et al. (0.7%).[23] Considering the known effect of the solvent in the relaxation of the excited state, we

Research Article
doi.org/10.1002/ceur.202300021

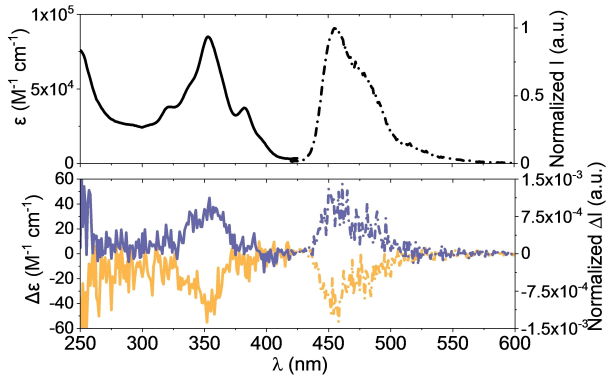

Figure 2. Top: UV/Vis absorption (solid line) and fluorescence spectra (λ_{exc} = 370 nm, dashed line) of **1** (CH_2Cl_2, *c.a.* 1.5×10^{-5} M). Bottom: ECD (left, 250–425 nm, solid line) and CPL spectra (right, 425–600 nm, dash line, λ_{exc} = 370 nm) of first (yellow, *M*-**1**) and second (blue, *P*-**1**) CSP-HPLC eluted fractions in CH_2Cl_2 (*c.a.* 1.5×10^{-5} M) at rt.

also analyzed the behavior of compound **1** in solvents with different polarity. Thus, we observed that φ_F increased in polar aprotic solvents such as MeCN and THF (9% and 11%, respectively, Table S1). Regarding the average fluorescence lifetime (τ_{av}), a good value of 17 ns in CH_2Cl_2 was observed, in the same range as all-carbon analogue (13 ns)[7] and higher than reported N-doped analogue (5 ns).[23] When the solvent was changed, the τ_{av} value was maintained, reaching a maximum of 22 ns for **1** in THF (Table S1). Thus, N-doping also means a slight improvement in the τ_{av} of these systems if we compare with the non-doped analogue (13 ns),[7] as long as an increase of the fluorescence quantum yields which implies an advantage considering sensing applications.

Additionally, we evaluated the electrochemical properties of **1** in MeCN (ca. 1.5 mM) by cyclic voltammetry (Figure S6). One partially reversible oxidation wave was observed, with a half-wave oxidation potential 0.89 V (vs $FeCp_2^+/FeCp_2$). Thus, the HOMO energy (–5.99 eV) is in the same range than HBC-*oct*-[5]helicenes.[7]

Enantiomeric resolution of racemic **1** was achieved by chiral stationary phase HPLC (CSP-HPLC) leading to two well-resolved peaks corresponding to the expected *M*/*P*-**1** enantiomers (Figure S1). Racemization studies of enantiopure **1** showed that neither racemization nor decomposition occurred when a solution of the second CSP-HPLC fraction in *n*-heptane was heated at 70 °C for 5 h. This means that we could establish a low limit of the corresponding isomerization barrier ($\Delta G^{\neq}$(T)) and ensure that the real value is higher than 27.0 kcal mol^{-1} at 343 K (Figure S5), which is already slightly higher than Rajca's *oct-[5]helicene* (24.4 kcal mol^{-1})[30] and Narita's HBC-*hept-[5]helicene* (25.4 kcal mol^{-1}),[31] but lower than the real value established for its all-carbon analogue (37.4 kcal mol^{-1}).[7]

The enantiomeric resolution and the adequate configurational stability allowed performing the study of the chiroptical properties both in absorption by the electronic circular dichroism (ECD) and in the emission by the circularly polarized luminescence (CPL). The ECD spectra in CH_2Cl_2 display mirror images for both enantiomers of **1** (Figure 2, bottom, solid lines), with a similar profile to the one reported by An.[23] The first CSP-HPLC eluted peak showed a negative Cotton effect at 352 nm ($|\Delta\varepsilon| = 55.1$ M^{-1} cm^{-1}, $|g_{abs}| = 6.5\times10^{-4}$; Figure 2, bottom, yellow solid line), very similar to the all-carbon HBC-*oct*-[5]helicene (7.6×10^{-4}). [7] The configurations of the two enantiomers were assigned by the comparison of the experimental ECD with the TD-DFT simulated ECD spectra (Figure S26). Thus, the first CSP-HPLC fraction of **1** was assigned to (*M*)-enantiomer and the second to the (*P*)-one. Besides, the theoretical study allowed us to establish the first transition $S_0\rightarrow S_1$, which is hardly perceptible in the experimental spectra, around 432 nm with a theoretical $|g_{abs}|$ of 1.1×10^{-3}.

On the other hand, having an enantiopure emissive compound in hands, we studied the CPL of the aza-HBC **1** in CH_2Cl_2. As expected, the CPL sign of each enantiomer gave the opposite and in good correlation with the sign of the theoretical longest wavelength ECD signal (Figure 2, bottom, dashed lines). The CPL spectra showed a maximum centered at 457 nm similar to the fluorescence spectrum, with a $|g_{lum}|$ value of 8.0×10^{-4} and a B_{CPL} (brightness for CPL defined as $\varepsilon\times\varphi_F\times g_{lum}/2$)[33] of 1.40 M^{-1} cm^{-1}. Hence, although similar $|g_{abs}|$ values were observed for both all-carbon and N-doped distorted HBCs, but remarkably the introduction of a nitrogen atom makes the molecule photostable permitting to measure the CPL, contrary to what happened in the all-carbon HBC analogue.[7]

As it was mentioned previously, motivated by the need for NIR organic materials including NIR chiroptical materials,[34] herein we develop a NIR chiroptical switch, in which the different states can be modulated by different stimuli such as redox or pH changes.

We started our study by examining the potential of an oxidant agent such as nitrosonium hexafluorophosphate, $NOPF_6$, (1.0 V in CH_2Cl_2 and 0.87 V MeCN vs $FeCp_2^+/FeCp_2$)[35] to oxidize **1** to its radical cation form [**1**]$^{\bullet+}$. First, the chemical titration upon addition of the oxidant was followed by means of ^{1}H NMR spectroscopy leading to a clear signals broadening (Figure S21), suggesting the formation of paramagnetic radical species. To confirm this hypothesis, the absorbance spectra of the oxidized species, both chemically (Figure 3A) and electrochemically (Figure 3B) generated, were measured in different solvents. In both approaches, a new near-infrared band in the range 700–900 nm (with the maximum at around 800 nm) appeared, which is attributed to the formation of radical species. The absorption spectrum obtained upon addition of $NOPF_6$ is not identical in the different solvents used, i.e. CH_2Cl_2, $CHCl_3$ and MeCN (Figure 3A) which suggests that the process depends on the standard reduction potential of $NOPF_6$ in each solvent, which would lead to distinct oxidized species of **1**. This can be clearly observed in the absorbance spectrum chemically generated in MeCN where the curve can be deconvoluted to three main bands centered at 727, 796 and 859 nm, indicating the simultaneous presence of three oxidized species (Figure 3A yellow and inset). In the case of the spectroelectrochemical measurements, again different solvents were used (Figure 3B) and the shape of the NIR absorption band varies in each case on the potential reached (Figures S18-S20). Moreover, only one clear isosbestic point is observed in all solvents, which indicate

Research Article
doi.org/10.1002/ceur.202300021

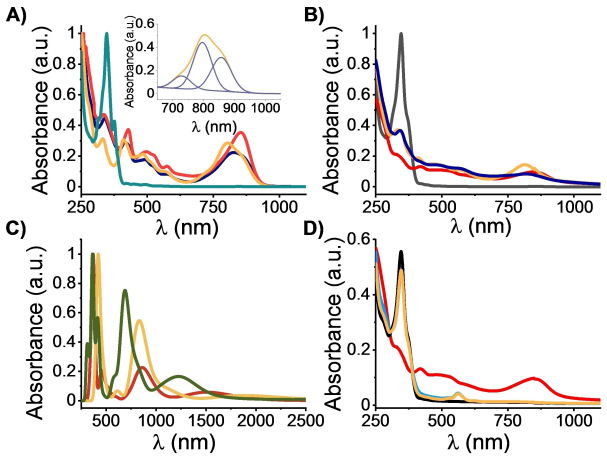

Figure 3. A) UV-Vis-NIR absorption spectra of **1** (6×10^{-5} M) in CH_2Cl_2 (cyan) and upon addition of $NOPF_6$ (excess) in: MeCN (yellow), CH_2Cl_2 (red), $CHCl_3$ (navy). Inset: Deconvolution of the UV-Vis-NIR absorption spectrum of the oxidized species of **1** in MeCN. B) Spectroelectrochemistry measurements of **1** (8×10^{-4} M) in different solvents: CH_2Cl_2 neutral (grey) and +1.3 V (red); MeCN +1.6 V (yellow) and $CHCl_3$ +1.5 V (blue). C) Simulated UV-Vis-NIR spectra of the different oxidized species of **1** in CH_2Cl_2: $[\mathbf{1}]^{\bullet+}$ (red), $[\mathbf{1}]^{2\bullet+}$ (yellow) and $[\mathbf{1}]^{2+}$ (green). D) Full reversible spectroelectrochemistry measurements of **1** (2×10^{-5} M) in CH_2Cl_2 at initial (black), 0 V (yellow), +1.3 V (red) and back to −0.2 V (cyan).

the equilibrium between oxidized and neutral species of **1** (Figure S20).

In order to shed light into the observed species, we performed geometrical optimization and theoretical UV/Vis spectra of the following possible oxidized species of **1**: radical cation $[\mathbf{1}]^{\bullet+}$, diradical dication $[\mathbf{1}]^{2\bullet+}$ and dication $[\mathbf{1}]^{2+}$. The theoretical results show that the three species are close in energy and present close absorption bands in the same region (Figure 3C). After comparing experimental and theoretical results we could tentatively assign the band close to 850 nm to $[\mathbf{1}]^{\bullet+}$, the band near to 800 nm to $[\mathbf{1}]^{2\bullet+}$ and, finally, the band proximate to 700 nm to $[\mathbf{1}]^{2+}$. The diradical dication species $[\mathbf{1}]^{2\bullet+}$ (triplet) is isoelectronic compared with the dication $[\mathbf{1}]^{2+}$ (singlet) and both species may evolve one into the other since the theoretical energies are quite similar for both species, only 0.14 kcal mol^{-1} approximately of difference between them.

Therefore, these results suggest that both methods, chemically and spectroelectrochemically, are appropriate to generate the radical species of **1**. Furthermore, we studied the redox switching and a fully reversibility of the process upon oxidation/reduction was observed in the first electrochemical cycle (Figure 3D). In the next cycles, reversibility is not complete probably due to some precipitation observed. In this sense, partial reversibility of the process upon chemical oxidation/reduction in MeCN is also observed although again the neutral specie is not fully recovered, probably due to the excess of reagents required (Figure S16).

Additionally, the results of the electron paramagnetic resonance (EPR) spectroscopy have confirmed the presence of radical species when **1** is oxidized chemically and spectroelectrochemically. The spectrum shows the coexistence of two species appearing at different *g*-factors corresponding to two different radical species (Figure 4A). Both show a three-line EPR spectrum due to the coupling of the electron/s with an N atom but with different coupling constants. One of them (*g*-factor = 2.0067, Figure 4A, in circles) presents a smaller coupling constant (a_N = 6.3 G) indicating that the electron is delocalised all over the molecule and the other (*g*-factor = 2.0042, Figure 4A, in asterisks) has a larger coupling constant (a_N = 30.1 G), indicating that the electron is localised on the nitrogen atom. To sum up, the NMR, UV/Vis and EPR studies are in good agreement with the formation of oxidized species observed of **1** upon oxidation.

Finally, considering that a new absorption band in the NIR region is easily generated upon oxidation, we added $NOPF_6$ in excess to enantiopure *M*/*P*-**1** to ensure their oxidation and measured ECD spectra of the resulting species. Both enantiomers display a new band around 800 nm with opposite sign that it is not observed in the neutral enantiomers matching the sign of the last band of the corresponding neutral enantiomer. This result is remarkable since it proofs that the chiroptical response of **1** in the NIR region can be modulated via redox changes.

Another approach to tune the properties of these compounds is to take advantage of the ability of the nitrogen atom to be sensitive to pH changes. In this sense, the optical properties of **1** were modulated in both absorbance and fluorescence by means of acid/base addition. In both cases, by adding trifluoroacetic acid (TFA), the signal decreased in the maximum, changing the color of the solution, from uncolored to pale yellow (Figure 5A/B, from yellow to red). In addition, an isosbestic point appears in the absorbance spectrum at almost 400 nm indicating the presence of another specie, highly probable the protonated **1**-H$^+$ (Figure 5A). Actually, a new band again in the NIR region is observed, very similar to the bands of the oxidized compounds (Figure 5A, inset). This new band in the NIR region is also well predicted by theoretical calculations (Figure S28). Notably, the addition of a base such as triethylamine (TEA) promoted the quasi or full recovery of the original spectra, in absorbance and fluorescence, respectively (Figure 5A/B, from red to green). Remarkably, several cycles were performed both in absorbance (Figure S23) and fluorescence, reaching one cycle in absorbance and three fully reversible cycles (acid-base) in fluorescence where the emission can be

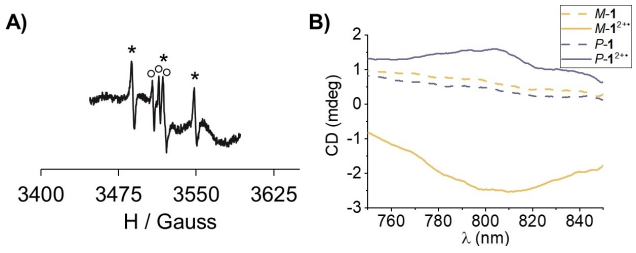

Figure 4. A) Two 3-line EPR spectra marked with asterisks (*g* = 2.0042, a_N = 30.1 G) and circles (*g* = 2.0067, a_N = 6.3 G) as contribution of two different oxidized (paramagnetic) species. The corresponding UV-Vis-NIR absorption spectrum of this sample is shown in Figure 3A-navy and inset. B) ECD spectra at the NIR region (750–850 nm) of *M*/P-**1** in CH_2Cl_2 (1.3×10^{-5} M) before (*M* in yellow; *P* in blue) and upon addition of an excess of $NOPF_6$ (*M* in yellow; *P* in blue).

Research Article
doi.org/10.1002/ceur.202300021

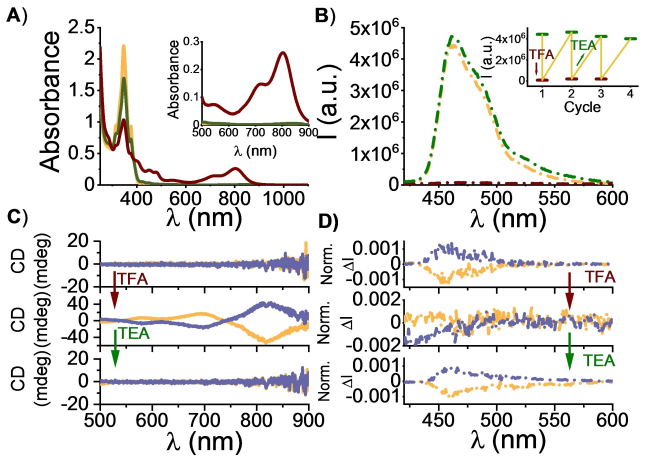

Figure 5. A) UV/Vis response of **1** in CH_2Cl_2 (yellow, 2.5×10^{-5} M) and after consecutive addition of acid (TFA, red) and base (TEA, green). B) Fluorescence spectra ($\lambda_{exc}=370$ nm) of **1** in CH_2Cl_2 (yellow, 2.5×10^{-5} M) and after consecutive addition of acid (TFA, red) and base (TEA, green). Inset: In situ *on-off* switching of the fluorescence emission of **1** in CH_2Cl_2 (2.5×10^{-5} M) after consecutive additions of acid (TFA, red) and base (TEA, green), $\lambda_{exc}=370$ nm. C) In situ *off-on* switching of the NIR-CD response of **1**: NIR-CD spectra of **1** in CH_2Cl_2 (8.5×10^{-5} M; *M*-**1**, yellow; *P*-**1**, blue, top) and after consecutive addition of acid (TFA, middle) and base (TEA, bottom). D) In situ *on-off* switching of the CPL emission of **1**: CPL spectra ($\lambda_{exc}=370$ nm) of **1** in CH_2Cl_2 (1.2×10^{-5} M; *M*-**1**, yellow; *P*-**1**, blue, top) and after consecutive addition of acid (TFA, middle) and base (TEA, bottom).

switched *on-off* just by adding acid-base (Figure 5B, inset). This reversibility of the system is also observed in ^{1}H NMR (Figure S24) where the addition of TFA may form the corresponding ammonium salt of **1**, widening the signals, and the subsequent incorporation of TEA returned to the initial neutral form of **1**.

Such interesting switching process was also interrogated for the chiroptical properties. To do that, both enantiomers of **1** were protonated under the same conditions as before and the ECD spectra of the new band was recorded in the NIR region (Figure 5C). Each enantiomer displays a new band around 800 nm with opposite sign that it is not present in the neutral enantiomers. In addition, the sign of the new band matches the sign of the last band of the corresponding neutral enantiomer with a $|g_{abs}|$ value of 1.2×10^{-3} at 813 nm, in concordance with the theoretical first transition of the neutral enantiomer. Those results are the proof-of-concept that N-doped distorted HBC **1** works as a NIR chiroptical switch via pH changes.

In terms of CPL, when the enantiomers of **1** are protonated, their CPL emission is quenched in the 400–700 nm and, remarkably, the TEA addition recovers the CPL activity, analogous to the fluorescence emission, confirming again the reversibility of the system (Figure 5D). Although we were not able to observe the emission of the new protonated species due to the available measuring range, those results show that the CPL emission can be easily switched *off-on* by consecutive acid-base additions.

Conclusions

In conclusion, another member of the chiral saddle-shaped HBC family has been synthesized, namely the aza-HBC-*oct*-[5]helicene. For the first time, the chiroptical properties of a chiral N-doped nanographene have been modulated by means of redox and pH changes as external stimuli. In both cases, a new absorption band appears in the NIR region after the addition of an oxidant or an acid, forming the corresponding oxidised or protonated species. Therefore, the chiroptical response of **1** can be modulated in the NIR in terms of CD. Analogously, the CPL response of **1** can be adjusted by changing the pH of the media. In both cases, the reversibility of the system was confirmed. Thus, these results demonstrate that compound **1** can act as a chiroptical switch. We consider that the multi optical response switching described here, in particular the chiroptical one, for which the NIR band can be modulated by changing the pH and the redox state is a remarkable achievement for future applications based on this phenomenon.

Acknowledgements

We acknowledge funding from FEDER(EDRF)/Junta de Andalucía-Consejería de Transformación Económica, Industria, Conocimiento y Universidades (B-FQM-428-UGR20), Plan Andaluz de Investigación, Desarrollo e Innovación2021 (P21-00133), Ministerio de Ciencia e Innovación (GENESIS PID2019-111682RB–I00, the PID2019-105622RB–I00), Generalitat de Catalunya (2021-SGR-00443) and the "Severo Ochoa" Programme for Centers of Excellence in R&D FUNFUTURE CEX2019-000917-S. L. H. thanks the Junta de Andalucía for a FPDI contract 2021 (PREDOC_00408). J. C.-T. thanks DOC-FAM fellowship (grant agreement Nr. 754397 through H2020-MSCA-COFUND-2016). J. C–T. is enrolled in the Materials Science PhD program of UAB. Authors thank the Centro de Servicios de Informática y Redes de Comunicación (CSIRC), UGR, for providing the computing time.

Conflict of Interests

The authors declare no conflict of interest.

Data Availability Statement

The data that support the findings of this study are available in the supplementary material of this article.

Keywords: chiroptical switch · circular dichroism · helicenes · hydrocarbons · N-doped · nanographenes

[1] S. H. Pun, Q. Miao, *Acc. Chem. Res.* **2018**, *51*, 1630–1642.
[2] Y. Zhong, B. Kumar, S. Oh, M. T. Trinh, Y. Wu, K. Elbert, P. Li, X. Zhu, S. Xiao, F. Ng, M. L. Steigerwald, C. Nuckolls, *J. Am. Chem. Soc.* **2014**, *136*, 8122–8130.

Research Article
doi.org/10.1002/ceur.202300021

[3] A. H. G. David, R. Casares, J. M. Cuerva, A. G. Campaña, V. Blanco, *J. Am. Chem. Soc.* **2019**, *141*, 18064–18074.
[4] a) V. Kiran, S. P. Mathew, S. R. Cohen, I. H. Delgado, J. Lacour, R. Naaman, *Adv. Mater.* **2016**, *28*, 1957–1962; b) R. Naaman, D. H. Waldeck, *Annu. Rev. Phys. Chem.* **2015**, *66*, 263–281.
[5] a) V. Berezhnaia, M. Roy, N. Vanthuyne, M. Villa, J. V. Naubron, J. Rodriguez, Y. Coquerel, M. Gingras, *J. Am. Chem. Soc.* **2017**, *139*, 18508–18511; b) T. Hosokawa, Y. Takahashi, T. Matsushima, S. Watanabe, S. Kikkawa, I. Azumaya, A. Tsurusaki, K. Kamikawa, *J. Am. Chem. Soc.* **2017**, *139*, 18512–18521; c) M. Roy, V. Berezhnaia, M. Villa, N. Vanthuyne, M. Giorgi, J. V. Naubron, S. Poyer, V. Monnier, L. Charles, Y. Carissan, D. Hagebaum-Reignier, J. Rodriguez, M. Gingras, Y. Coquerel, *Angew. Chem. Int. Ed.* **2020**, *59*, 3264–3271, *Angew. Chem.* **2020**, *132*, 3290–3297; d) G. Báti, D. Csókás, T. Yong, S. M. Tam, R. R. S. Shi, R. D. Webster, I. Pápai, F. García, M. C. Stuparu, *Angew. Chem. Int. Ed.* **2020**, *59*, 21620–21626, *Angew. Chem.* **2020**, *132*, 21804–21810; e) I. R. Márquez, S. Castro-Fernández, A. Millán, A. G. Campaña, *Chem. Commun.* **2018**, *54*, 6705–6718; f) A. Borissov, Y. K. Maurya, L. Moshniaha, W.-S. Wong, M. Zyla-Karwowska, M. Stępień, *Chem. Rev.* **2022**, *122*, 565–788; g) T. Fujikawa, Y. Segawa, K. Itami, *J. Org. Chem.* **2017**, *82*, 7745–7749; h) J. Ma, Y. Fu, E. Dmitrieva, F. Liu, H. Komber, F. Hennersdorf, A. A. Popov, J. J. Weigand, J. Liu, X. Feng, *Angew. Chem. Int. Ed.* **2020**, *59*, 5637–5642; *Angew. Chem.* **2020**, *132*, 5686–5691.
[6] I. R. Márquez, N. Fuentes, C. M. Cruz, V. Puente-Muñoz, L. Sotorrios, M. L. Marcos, D. Choquesillo-Lazarte, B. Biel, L. Crovetto, E. Gómez-Bengoa, M. T. González, R. Martin, J. M. Cuerva, A. G. Campaña, *Chem. Sci.* **2017**, *8*, 1068–1074.
[7] M. A. Medel, R. Tapia, V. Blanco, D. Miguel, S. P. Morcillo, A. G. Campaña, *Angew. Chem. Int. Ed.* **2021**, *60*, 6094–6100; *Angew. Chem.* **2021**, *133*, 6159–6165.
[8] M. A. Medel, C. M. Cruz, D. Miguel, V. Blanco, S. P. Morcillo, A. G. Campaña, *Angew. Chem. Int. Ed.* **2021**, *60*, 22051–22056; *Angew. Chem.* **2021**, *133*, 22222–22227.
[9] J. M. Fernández-García, P. Izquierdo-García, M. Buendía, S. Filippone, N. Martín, *Chem. Commun.* **2022**, *58*, 2634–2645.
[10] a) C. M. Cruz, I. R. Márquez, I. F. A. Mariz, V. Blanco, C. Sánchez-Sánchez, J. M. Sobrado, J. A. Martín-Gago, J. M. Cuerva, E. Maçôas, A. G. Campaña, *Chem. Sci.* **2018**, *9*, 3917–3924; b) C. M. Cruz, I. R. Márquez, S. Castro-Fernández, J. M. Cuerva, E. Maçôas, A. G. Campaña, *Angew. Chem. Int. Ed.* **2019**, *58*, 8068–8072; *Angew. Chem.* **2019**, *131*, 8152–8156.
[11] C. M. Cruz, S. Castro-Fernández, E. Maçôas, J. M. Cuerva, A. G. Campaña, *Angew. Chem. Int. Ed.* **2018**, *57*, 14782–14786, *Angew. Chem. Int. Ed.* **2018**, *130*, 14998–15002.
[12] a) M. Stępień, E. Gońka, M. Żyła, N. Sprutta, *Chem. Rev.* **2017**, *117*, 3479–3716; b) X. Y. Wang, X. Yao, A. Narita, K. Müllen, *Acc. Chem. Res.* **2019**, *52*, 2491–2505.
[13] S. Muhammad, A. R. Chaudhry, A. Irfan, A. G. Al-Sehemi, *RSC Adv.* **2017**, *7*, 36632–36643.
[14] E. S. Gauthier, R. Rodríguez, J. Crassous, *Angew. Chem. Int. Ed.* **2020**, *59*, 22840–22856; *Angew. Chem.* **2020**, *132*, 23036–23052.
[15] P. Nitschke, B. Jarząbek, A. E. Bejan, M. D. Damaceanu, *J. Phys. Chem. B* **2021**, *125*, 8588–8600.
[16] L. Zhou, B. Wu, Y. Chen, J. Gong, J. Wang, G. Dai, C. Chi, Q. Wang, *Org. Lett.* **2021**, *23*, 8640–8644.
[17] S. M. Draper, D. J. Gregg, R. Madathil, *J. Am. Chem. Soc.* **2002**, *124*, 3486–3487.
[18] D. Reger, K. Schöll, F. Hampel, H. Maid, N. Jux, *Chem. Eur. J.* **2021**, *27*, 1984–1989.
[19] a) M. Zyła, E. Gońka, P. J. Chmielewski, J. Cybińska, M. Stępień, *Chem. Sci.* **2016**, *7*, 286–294; b) Y. Sasaki, M. Takase, T. Okujima, S. Mori, H. Uno, *Org. Lett.* **2019**, *21*, 1900–1903; c) H. Uno, M. Ishiwata, K. Muramatsu, M. Takase, S. Mori, T. Okujima, *Bull. Chem. Soc. Jpn.* **2019**, *92*, 973–981.
[20] a) M. Takase, V. Enkelmann, D. Sebastiani, M. Baumgarten, K. Müllen, *Angew. Chem. Int. Ed.* **2007**, *46*, 5524–5527; b) M. Takase, T. Narita, W. Fujita, M. S. Asano, T. Nishinaga, H. Benten, K. Yoza, K. Müllen, *J. Am. Chem. Soc.* **2013**, *135*, 8031–8040.
[21] T. Kirschbaum, F. Rominger, M. Mastalerz, *Chem. Eur. J.* **2020**, *26*, 14560–14564.
[22] R. K. Dubey, M. Melle-franco, A. Mateo-Alonso, *J. Am. Chem. Soc.* **2022**, *144*, 2765–2774.
[23] P. An, R. Li, B. Ma, R. Y. He, Y. K. Zhang, M. J. Xiao, B. Zhang, *Angew. Chem. Int. Ed.* **2021**, *60*, 24478–24483; *Angew. Chem.* **2021**, *133*, 24683–24688.
[24] a) J. K. Zak, M. Miyasaka, S. Rajca, M. Lapkowski, A. Rajca, *J. Am. Chem. Soc.* **2010**, *132*, 3246–3247; b) T. Biet, A. Fihey, T. Cauchy, N. Vanthuyne, C. Roussel, J. Crassous, N. Avarvari, *Chem. Eur. J.* **2013**, *19*, 13160–13167; c) D. Schweinfurth, M. Zalibera, M. Kathan, C. Shen, M. Mazzolini, N. Trapp, J. Crassous, G. Gescheidt, F. Diederich, *J. Am. Chem. Soc.* **2014**, *136*, 13045–13052.
[25] T. M. Liu, J. Conde, T. Lipiński, A. Bednarkiewicz, C. C. Huang, *NPG Asia Mater.* **2016**, *8*, e295.
[26] a) K. Takaishi, M. Yasui, T. Ema, *J. Am. Chem. Soc.* **2018**, *140*, 5334–5338; b) H. Isla, N. Saleh, J.-K. Ou-Yang, K. Dhbaibi, M. Jean, M. Dziurka, L. Favereau, N. Vanthuyne, L. Toupet, B. Jamoussi, M. Srebro-Hooper, J. Crassous, *J. Org. Chem.* **2019**, *84*, 5383–5393; c) C. Maeda, K. Nagahata, T. Shirakawa, T. Ema, *Angew. Chem. Int. Ed.* **2020**, *59*, 7813–7817; *Angew. Chem.* **2020**, *132*, 7887–7891; d) H. Isla, M. Srebro-Hooper, M. Jean, N. Vanthuyne, T. Roisnel, J. L. Lunkley, G. Muller, J. A. Gareth Williams, J. Autschbach, J. Crassous, *Chem. Commun.* **2016**, *52*, 5932–5935; e) N. Saleh, B. Moore II, M. Srebro, N. Vanthuyne, L. Toupet, J. A. Gareth Williams, C. Roussel, K. K. Deol, G. Muller, J. Autschbach, M. Crassous, *Chem. Eur. J.* **2015**, *21*, 1673–1681; f) H. Sakai, T. Kubota, J. Yuasa, Y. Araki, T. Sakanoue, T. Takenobu, T. Wada, T. Kawai, T. Hasobe, *Org. Biomol. Chem.* **2016**, *14*, 6738–6743; g) T. Otani, A. Tsuyuki, T. Iwachi, S. Someya, K. Tateno, H. Kawai, T. Saito, K. S. Kanyiva, T. Shibata, *Angew. Chem. Int. Ed.* **2017**, *56*, 3906–3910; *Angew. Chem.* **2017**, *129*, 3964–3968; h) S. Pascal, C. Besnard, F. Zinna, L. D. Rari, B. L. Guennic, D. Jacquemin, J. Lacour, *Org. Biomol. Chem.* **2016**, *14*, 4590–4594; i) X. Gong, C. Li, Z. Cai, X. Wan, H. Qian, G. Yang, *J. Org. Chem.* **2022**, *87*, 8406–8412.
[27] a) L. Pospíšil, L. Bednárová, P. Štěpánek, P. Slavíček, J. Vávra, M. Hromadová, H. Dlouhá, J. Tarábek, F. Teplý, *J. Am. Chem. Soc.* **2014**, *136*, 10826–10829; b) K. Xu, Y. Fu, Y. Zhou, F. Hennersdorf, P. Machata, I. Vincon, J. J. Weigand, A. A. Popov, R. Berger, X. Feng, *Angew. Chem. Int. Ed.* **2017**, *56*, 15876–15881; *Angew. Chem.* **2017**, *129*, 16092–16097; c) S. Kasemthaveechok, L. Abella, M. Jean, M. Cordier, T. Roisnel, N. Vanthuyne, T. Guizouarn, O. Cador, J. Autschbach, J. Crassous, L. Favereau, *J. Am. Chem. Soc.* **2020**, *142*, 20409–20418; d) S. Kasemthaveechok, L. Abella, M. Jean, M. Cordier, N. Vanthuyne, O. Cador, J. Autschbach, J. Crassous, L. Favereau, *J. Am. Chem. Soc.* **2022**, *144*, 7253–7263.
[28] a) C. Shen, G. Loas, M. Srebro-Hooper, N. Vanthuyne, L. Toupet, O. Cador, F. Paul, J. T. L. Navarrete, F. J. Ramírez, B. Nieto-Ortega, J. Casado, J. Autschbach, M. Vallet, J. Crassous, *Angew. Chem. Int. Ed.* **2016**, *55*, 8062–8066; *Angew. Chem.* **2016**, *128*, 8194–8198; b) C. Shen, X. He, L. Toupet, L. Norel, S. Rigaut, J. Crassous, *Organometallics* **2018**, *37*, 697–705; c) E. Anger, M. Srebro, N. Vanthuyne, L. Toupet, S. Rigaut, C. Roussel, J. Autschbach, J. Crassous, R. Réau, *J. Am. Chem. Soc.* **2012**, *134*, 15628–15631.
[29] L. Zhai, R. Shukla, R. Rathore, *Org. Lett.* **2009**, *11*, 3474–3477.
[30] A. Rajca, A. Safronov, S. Rajca, J. Wongsriratanakul, *J. Am. Chem. Soc.* **2000**, *122*, 3351–3357.
[31] Z. Qiu, S. Asako, Y. Hu, C. W. Ju, T. Liu, L. Rondin, D. Schollmeyer, J. S. Lauret, K. Müllen, A. Narita, *J. Am. Chem. Soc.* **2020**, *142*, 14814–14819.
[32] C. Bazzini, S. Brovelli, T. Caronna, C. Gambarotti, M. Giannone, P. Macchi, F. Meinardi, A. Mele, W. Panzeri, F. Recupero, A. Sironi, R. Tubino, *Eur. J. Org. Chem.* **2005**, 1247–1257.
[33] L. Arrico, L. Di Bari, F. Zinna, *Chem. Eur. J.* **2021**, *27*, 2920–2934.
[34] S. Míguez-Lago, I. F. A. Mariz, M. A. Medel, J. M. Cuerva, E. Maçôas, C. M. Cruz, A. G. Campaña, *Chem. Sci.* **2022**, *13*, 10267–10272.
[35] N. G. Connelly, W. E. Geiger, *Chem. Rev.* **1996**, *96*, 877–910.

Manuscript received: April 1, 2023
Version of record online: July 28, 2023